Available online at www.sciencedirect.com
SCIENCE DIRECT®
Aerospace Science and Technology 9 (2005) 19–29
Aerospace Science and Technology
www.elsevier.com/locate/aescte

# An inverse design method for engine nacelles and wings

# Ein inverses Verfahren zum Entwurf von Triebwerksgondeln und Tragflügeln

Roland Wilhelm [1]

*DLR, Institute of Aerodynamics and Flow Technology, 38108 Braunschweig, Germany*

Received 10 June 2004; received in revised form 11 August 2004; accepted 9 September 2004

Available online 26 October 2004

**Abstract**

The application of an iterative design method allows the aerodynamic design of engine nacelles and wings being part of complex aircraft configurations. The method couples a flow solver for the solution of the Euler/Navier–Stokes equations on unstructured grids with a design algorithm which solves the transonic potential equation for small perturbations via an inverse formulation. The accuracy and robustness of the design method is investigated for redesigns of engine nacelles and wings. Several design cases demonstrate the efficient application of the method for the aerodynamic design of installed engine nacelles and wings under influence of complex aircraft configurations. One application shows that the method also can be used to minimize aerodynamic installation effects resulting from the engine integration process by sole nacelle or wing contour shaping. A general design methodology for engine nacelles is derived which allows to take into account all aerodynamic effects on complex configurations during the design process.
© 2004 Elsevier SAS. All rights reserved.

**Zusammenfassung**

Durch Anwendung eines iterativen Entwurfsverfahrens werden an komplexen Konfigurationen installierte Flügel und Triebwerksgondeln aerodynamisch entworfen. Das Verfahren koppelt ein Strömungsberechnungsverfahren für unstrukturierte Gitter zur Lösung der Euler/Navier–Stokes Gleichungen mit einem Entwurfsalgorithmus, welcher die transsonische Potentialgleichung über einen inversen Ansatz löst. Die Genauigkeit und Robustheit des Verfahrens wird für verschiedene Nachentwürfe von Triebwerksgondeln und Flügeln untersucht. Weiterhin zeigen Entwürfe von Triebwerksgondeln und Flügeln, dass das Verfahren im Rahmen des aerodynamischen Entwurfs an komplexen Konfigurationen effizient eingesetzt werden kann. Neben dem direkten Entwurf wird demonstriert, dass das Verfahren auch zur Verringerung von aerodynamischen Installationseffekten durch Änderung der Flügel-bzw. Triebwerksgondelkontur bei der Triebwerksintegration erfolgreich angewendet werden kann. Eine allgemeine Entwurfsmethodik für Triebwerksgondeln wird vorgestellt, die es ermöglicht, alle an komplexen Konfigurationen auftretenden aerodynamischen Effekte im Entwurfsprozess zu berücksichtigen.
© 2004 Elsevier SAS. All rights reserved.

*Keywords:* Inverse method; Wing design; Nacelle design; Transonic; Unstructured grid

*Schlüsselwörter:* Inverses Verfahren; Flügelentwurf; Triebwerksgondelentwurf; Transsonisch; Unstrukturierte Gitter

## 1. Introduction

The aerodynamic design of aircraft configurations is a discipline involving extensive use of numerical design and optimization methods. For complete new designs the aim is

*E-mail address:* rolandcw@web.de (R. Wilhelm).
[1] Tel. +49 (0)531 295 2283; Fax +49 (0)531 295 2320.

1270-9638/$ – see front matter © 2004 Elsevier SAS. All rights reserved.
doi:10.1016/j.ast.2004.09.002

**Nomenclature**

| | | | |
|---|---|---|---|
| $c$ | Chord length | $y^+$ | Dimensionless wall distance |
| $c_P$ | Pressure coefficient | $x, y, z$ | Cartesian coordinates |
| $C_D$ | Total drag coefficient | $\Delta z$ | Geometry difference |
| $C_L$ | Total lift coefficient | $\alpha$ | Angle of attack |
| $D$ | Scaling factor | $\beta$ | Transformation factor |
| $K$ | Transonic similarity parameter | $\varepsilon_{\text{Fan}}$ | Stream tube area ratio |
| $M_\infty$ | Free stream Mach number | $\eta$ | Spanwise coordinate |
| $r$ | Nacelle radius | $\Theta$ | Circumferential section angle |
| $\Delta r$ | Radial geometry difference | $\kappa$ | Ratio of specific heats |
| Re | Reynolds number | $\phi$ | Velocity potential |
| $U_\infty$ | Free stream velocity | $\Phi$ | Perturbation velocity potential |

to find a configuration close to the overall aircraft optimum while given constraints may be traded off against constraints of other disciplines. When doing a reengineering of an existing aircraft for increasing its performance, a so-called retrofit or derivative, numerous fixed constraints have to be satisfied. Both tasks need design methods which are able to precisely fulfill these demands.

Two well-known numerical methods exist for the aerodynamic design of aircraft components like the wing or nacelle, or of complete aircraft configurations: optimization techniques and inverse design techniques. Optimization techniques often focus on global parameters like total lift or drag, the object of the optimization. The aim is to minimize the objective function by varying defined design variables. Depending on the optimization strategy and the number of design variables an optimization can become very time consuming.

In contrast, inverse design methods give the opportunity to influence the local flow field surrounding the configuration to be designed. As the name *inverse* indicates these methods change the workflow direction of the typical analysis problem where a geometry is given and a flow field solution is desired. Using a user specified surface pressure distribution (the target) these methods aim at generating a geometry which satisfies this target. Inverse methods convert a surface pressure difference into a geometry difference. This is followed by an analysis step in which a flow field solution of the configuration including the geometry differences is calculated. Subsequent iterations between these two steps yield a new design solution. Obviously, this method requires some expert knowledge about the general flow regime and the flow physics. In addition there is no guarantee that the specified pressure distribution will yield a physical solution.

Several inverse design methods exist in the field of aerodynamics. The method of Campbell and Smith [4] converts the surface pressure difference between the actual and the target pressure distribution into a change in surface curvature. Integrating the new curvature distribution leads to a new surface. Besides the design of airfoils and wings, this method has been applied to inverse designs of nacelles, winglets and complete aircraft configurations [2,5,11,14]. Malone et al. [12] use an elastic surface method to design wing and nacelle configurations. The original method as derived by Garabedian et al. [9] relates differences in surface velocities between target and actual geometry to derivatives of the surface with respect to a pseudo time and a streamwise coordinate. Thus, the surface varies in time until the surface velocity differences approach zero.

A well-known aerodynamic design tool is the inverse design method of Takanashi [15]. The inverse formulation of the transonic small perturbation equation is used to convert surface pressure differences between a user-prescribed target pressure distribution and the actual pressure distribution into geometry differences. Applying this method in an iterative approach, a geometry can be generated which fulfills the target pressure distribution. The method has been applied for various airfoil, wing and nacelle design cases [8,13].

The present paper uses a modular Inverse Design System (Wilhelm [16]). The algorithm couples the inverse design method developed by Takanashi [15] and extended by Bartelheimer [1] with the DLR TAU code [10].

## 2. Numerical method

The Inverse Design System used in this paper [16] links an inverse design method formerly combined with a block-structured flow solver to the DLR TAU code [10], a flow solver for the solution of the Euler/Navier–Stokes equations on unstructured grids. Utilizing the unstructured grid approach a higher flexibility concerning configuration changes can be achieved because the time consuming initial grid generation process known for block-structured grids around complex configurations can be reduced significantly. Fig. 1 gives an overview of the numerical method. As can be seen the design system includes four main modules: the *flow solver*, the *solution interpolation*, the *inverse design*, and the *grid deformation* module.

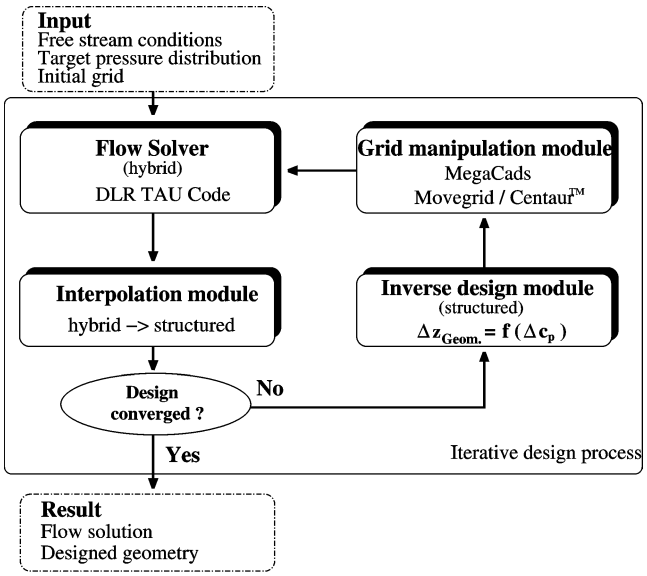


Fig. 1. Flow chart of Inverse Design System.

Starting with the initial geometry the analysis step is done resulting in a flow field solution of the starting configuration. The interpolation module transfers the necessary flow field solution data from the surface grid consisting of triangles to the design surface grid (a structured surface grid consisting of quadrilaterals). The design module calculates the difference between the actual and the target pressure distribution and converts it into a geometry difference. During this design step the aircraft component (i.e. nacelle or wing) is treated as an isolated geometric component without any further influence from the remaining aircraft configuration. Finally, the calculated geometry difference is introduced into the finite-volume grid of the last flow field analysis to give a modified grid for the next analysis step.

The following subsections will give a detailed explanation of the conceptual and numerical methods used in the modules.

### 2.1. Flow solver

The flow solver used within the Inverse Design System is the DLR TAU Code [10]. The code solves the three-dimensional Euler/Navier–Stokes equations using control volumes consisting of triangular or quadrilateral faces. The discretization in space is done using a central differencing scheme. Therefore, additional second and fourth order dissipative terms are added to the flux balance. The time integration is performed using a 3-stage Runge–Kutta scheme. Acceleration techniques including multigrid and local time stepping are applied, too.

For the results presented in this article, the flow field calculations performed within the design loop are done in an inviscid flow regime. Therefore, all primary grids consist of tetrahedral control volumes only. The reason for this is the time saving gained by applying the Euler instead of the Navier–Stokes equations within the iterative design loop. It has to be mentioned that the main flow phenomena at cruise conditions are not exactly resolved in an inviscid flow regime. In general, since the TAU code solves the three-dimensional Euler/Navier–Stokes equations, the Inverse Design System is capable of handling both viscous and inviscid flow field solutions. A trade-off has to be done by the user between physical simulation accuracy and numerical simulation effort. Nevertheless, various design improvements like shock strength reduction can be achieved in an inviscid flow regime. Doing so, the inverse design run should be followed by a final design check in a viscous flow regime in order to estimate the configuration improvements.

### 2.2. Solution interpolation

The solution interpolation transfers the data of the flow field solution from the unstructured surface grid (consisting of triangles) to the design surface grid (a structured surface grid consisting of quadrilaterals). During this interpolation step only surface pressure values are taken into account since all necessary flow field information for the design method is contained in this data. The solution interpolation is subdivided into cuts through the surface. For a constant angle in circumferential direction or a constant spanwise coordinate a cut plane is defined which extracts the solution data of the edges of the surface triangles which cut the plane. Since the structured surface grid consists of grid lines of constant circumferential angle or spanwise coordinate, too, the extracted cut data is splined in streamwise direction onto the structured surface points within each section using a cubic spline interpolation.

### 2.3. Inverse method

The inverse design method presented in this paper is based on an iterative "residual-correction" type approach. The residual $\Delta c_P$ being the pressure difference between the actual and the target pressure distribution is used to calculate a geometry difference $\Delta z$. The correction step is done by solving an inverse formulation of the transonic small perturbation equation (TSP-equation) as derived by Takanashi [15].

The three-dimensional potential equation can be written in terms of a perturbation velocity potential $\Phi$ as

$$(1 - M_\infty^2)\Phi_{xx} + \Phi_{yy} + \Phi_{zz} = K \cdot \Phi_x \Phi_{xx}$$
$$\text{with } K = (\kappa + 1)M_\infty^2, \tag{1}$$

where $\Phi$ is defined as

$$\phi = U_\infty(x + \Phi). \tag{2}$$

Two simplified boundary conditions can be applied to Eq. (1). The first one applies the tangency condition on the surface while the second one is a simplified pressure relation

$$\Phi_z(x, y, \pm 0) = \frac{\partial z(x, y, \pm 0)}{\partial x}, \tag{3}$$

$$\Phi_x(x, y, \pm 0) = -\frac{c_P(x, y, \pm 0)}{2}. \tag{4}$$

The $\pm$ sign denotes the upper or lower side of the surface. In order to eliminate the dependency on the free stream Mach number in $\beta^2 = 1 - M_\infty^2$ a Prandtl–Glauert transformation is performed and new coordinates $\bar{x}$, $\bar{y}$, $\bar{z}$ are introduced. Assuming that for an initial geometry $\bar{z}(\bar{x}, \bar{y}, \pm 0)$ a flow field solution $\overline{\Phi}(\bar{x}, \bar{y}, \bar{z})$ exists, a differential perturbation potential $\Delta\overline{\Phi}(\bar{x}, \bar{y}, \bar{z})$ can be introduced into Eq. (1)

$$\Delta\overline{\Phi}_{\bar{x}\bar{x}} + \Delta\overline{\Phi}_{\bar{y}\bar{y}} + \Delta\overline{\Phi}_{\bar{z}\bar{z}} = \frac{\partial}{\partial x}\left[\frac{1}{2}(\overline{\Phi}_{\bar{x}} + \Delta\overline{\Phi}_{\bar{x}})^2 - \frac{1}{2}(\overline{\Phi}_{\bar{x}})^2\right]. \tag{5}$$

The two boundary conditions of Eqs. (3) and (4) become

$$\Delta\overline{\Phi}_{\bar{z}}(\bar{x}, \bar{y}, \pm 0) = \frac{K}{\beta^3}\frac{\partial\Delta\bar{z}(\bar{x}, \bar{y}, \pm 0)}{\partial\bar{x}}, \tag{6}$$

$$\Delta\overline{\Phi}_{\bar{x}}(\bar{x}, \bar{y}, \pm 0) = -\frac{K}{2\beta^2}\Delta c_P(\bar{x}, \bar{y}, \pm 0). \tag{7}$$

The pressure difference $\Delta c_P(\bar{x}, \bar{y}, \pm 0)$ in Eq. (7) can be computed using the calculated flow solution and the prescribed target pressure distribution

$$\Delta c_P = c_P^{\text{target}} - c_P^{\text{calculated}}. \tag{8}$$

The right hand side of Eq. (5) is known using Eqs. (4) and (7). Eq. (5) can be solved for the unknown geometry difference $\bar{z}(\bar{x}, \bar{y}, \pm 0)$ using Green's theorem. In a final step the computed geometry correction has to be transfered back into the original $x$, $y$, $z$-coordinate system.

The TSP-equation does not distinguish between flow regimes of elliptic (subsonic) or hyperbolic (supersonic) character. Therefore, the design solution may not converge in transonic flow regions since a stable solution scheme has to use some upwind biased formulation in hyperbolic regions in order to cover the correct flow physics. Bartelheimer [1] introduced a stabilizing upwind-discretization scheme into the methods original Eq. (5) which is applied in hyperbolic regions. Therefore, the modified governing design equation is

$$\Delta\overline{\Phi}_{\bar{x}\bar{x}} + \Delta\overline{\Phi}_{\bar{y}\bar{y}} + \Delta\overline{\Phi}_{\bar{z}\bar{z}} = \frac{\partial}{\partial x}\left[\frac{1}{2}(\overline{\Phi}_{\bar{x}} + \Delta\overline{\Phi}_{\bar{x}})^2 - \frac{1}{2}(\overline{\Phi}_{\bar{x}})^2 + D\cdot\Delta\bar{x}\Delta\overline{\Phi}_{\bar{x}\bar{x}}(1 - \overline{\Phi}_{\bar{x}} - \Delta\overline{\Phi}_{\bar{x}})\right]. \tag{9}$$

For transonic flow fields with low supersonic velocities the factor $D$ is set to 1.0. In case of flow regimes with distinct supersonic flow velocities the factor $D$ has to be increased up to a value of 10.0 in order to achieve a converged design solution.

The formulas above and their coordinate system are given in a general formulation applicable for wing design, i.e. the $x$-coordinate running in streamwise, the $y$-coordinate running in spanwise direction and the $z$-coordinate running in the resulting direction for a right-hand side coordinate system. In case of a nacelle design run, the coordinate system is temporary changed with $y$ now being the circumferential coordinate direction and $z$ running in the radial direction (both taken with respect to the engine axis). The $x$-coordinate remains the streamwise direction. In essence, for nacelle inverse design a quasi-circular wing is formed whose inner rear end is not considered as part of the computational domain. The geometry difference $\Delta z$ therefore is a radial geometry difference $\Delta r$.

Before the calculated geometry differences are added to the actual design surface, they are smoothed in streamwise and spanwise or circumferential direction using a Bézier curve technique. The design procedure ensures that the nacelle or wing planform remain constant throughout the whole design process. Two fixed points of the nacelle are the fan radius and the fan nozzle radius. For a wing design with a constant twist distribution, the leading and trailing edge lines are fixed. The result of the inverse design module is a modified geometry in terms of thickness and chamber.

### 2.4. Grid deformation

The finite-volume grid deformation is necessary in order to generate a computational grid of the modified configuration. Besides the possibility to generate the finite-volume grid in each design iteration from scratch, the more efficient way is to apply a grid deformation method which fits an existing grid to a modified configuration. Also, since only one baseline grid consisting of a constant number of grid points is used for all flow field calculations in the design loop, the restart ability of the flow solver TAU contributes to the systems overall efficiency, too.

In order to fulfill the above mentioned demands, the grid generation package *Centaur* [6] is used to generate the initial finite-volume grid for the starting configuration. *Centaur* is capable of designing hybrid grids consisting of prismatic, hexahedral, pyramidal or tetrahedral control volumes. An initial grid is generated before the main inverse design run is started. Then, within each design cycle, a grid deformation algorithm is used to fit the initial grid to the modified configuration. Since the initial grid will be the baseline finite-volume grid for all flow field calculations performed in the design loop, its quality should be analyzed carefully before a design run.

The grid deformation step in the design loop is divided into two steps. In the first step the DLR grid generation package MegaCads [3] is used to merge the designed surface (i.e. the isolated nacelle or wing) with the remaining aircraft components like fuselage and pylon. Especially, due to the modified surface, new intersection lines between pylon and nacelle or wing and fuselage/pylon are calculated. In order to result into a water-tight domain, farfield and symmetry plane are added, too. Now, the complete configuration is represented by trimmed surfaces. The second step applies the finite-volume grid deformation. The *Centaur* grid gener-

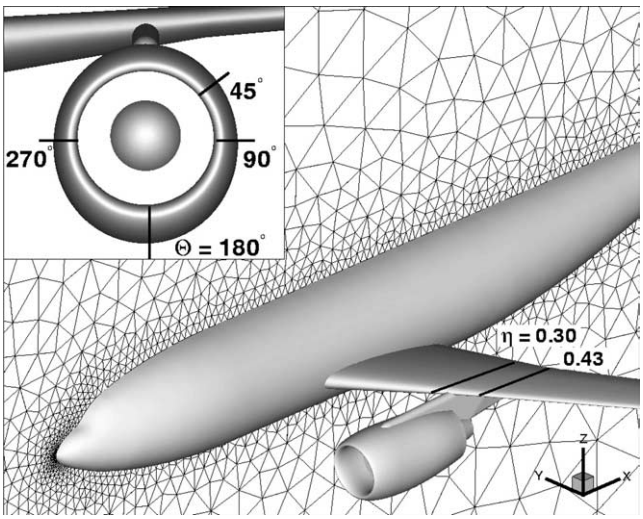


Fig. 2. DLR ALVAST-VHBR configuration.

ation package includes a grid deformation algorithm which fits an existing grid to a modified configuration. The algorithm moves the surface grid points of the finite-volume grid located at a former position onto the new surface. After this surface point mapping, the surrounding interior field points are moved in a decaying manner depending on their individual distance from the modified surface. Applying this algorithm results in a grid which will be used for the following flow field analysis in the next design iteration.

## 3. Results

In this section results will be presented of the application of the Inverse Design System. The examples include nacelle and wing design cases. In addition, an application is presented which primarily focuses on the reduction of aerodynamic engine integration effects by shaping the wing or nacelle contour.

### 3.1. Nacelle redesign

The first test case is a redesign of an existing wing-mounted engine nacelle. Redesign cases are used to test the correct formulation and the quality of a numerical design algorithm. Since the solution of a redesign task is known by definition, it can be compared against the resulting solution of the design algorithm. Also, a redesign case ensures that no unphysical target pressure distribution is prescribed, a so called "ill-posed" design problem.

The aircraft used for the redesign of a wing-mounted engine nacelle is the DLR ALVAST configuration, a generic twin engine subsonic transport aircraft (see Fig. 2). The original model, the target configuration, is equipped with a non-axi-symmetric VHBR (very high bypass ratio) engine nacelle. The starting geometry for the nacelle redesign is a nacelle of the same planform as the target. Its shape is setup by the scaled profiles of the target nacelle at $\theta = 90°$ (horizontal plane) only. In essence, when neglecting the intake droop angle, the initial nacelle would be axi-symmetric.

The free stream and main engine parameters for this nacelle redesign are the Mach number $M_\infty = 0.75$, the angle of attack $\alpha = 0.50°$ and the stream tube area ratio $\varepsilon_{\text{Fan}} = 0.92$. The flow field calculations are performed assuming an inviscid flow regime. Fig. 3 shows surface pressure distributions and nacelle profiles in two circumferential sections at $\theta = 45°$ and 180° (corresponding to the outboard upper and the bottom section, respectively). As can be seen the prescribed target pressure distributions are met in both sections by the pressure distributions of the designed contours. Also, the designed nacelle contours match the target contours well. As a result of the redesign, the thickness in the bottom part of the nacelle has considerably increased.

The convergence history of this redesign case is shown in Fig. 4. Within the first 1200 time steps the flow field solution of the starting configuration converges to steady state. This solution is generated before the iterative design run. Starting at time step 1200, the average density residual $\|\delta\rho/\delta t\|$ shows that within each design cycle (of a total of 30 cycles)

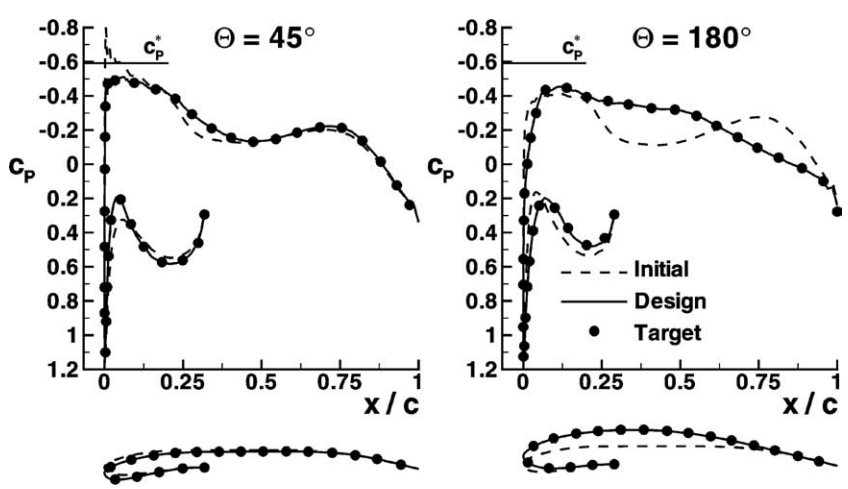


Fig. 3. Redesign of a wing-mounted engine nacelle: surface pressure distributions and nacelle profiles.

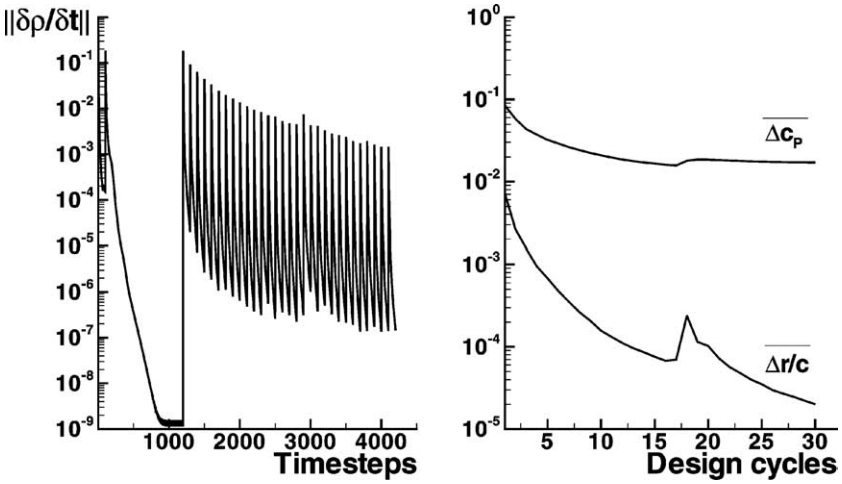


Fig. 4. Redesign of a wing-mounted engine nacelle: convergence history of flow field and design solutions.

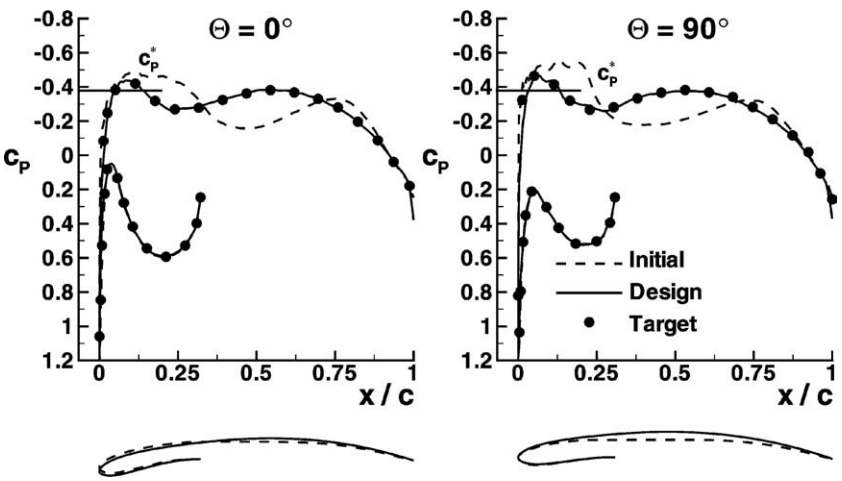


Fig. 5. Design of an isolated HLF engine nacelle: surface pressure distributions and nacelle profiles.

a converged flow field solution is gained within 100 time steps. As an indication for the convergence of the redesign task, plots of the average surface pressure difference $\overline{\Delta c_P}$ and of the average geometry difference $\overline{\Delta r/c}$ are shown, too. With each design cycle both values decrease which indicates that the redesign solution approaches the targeted nacelle contour. One oscillation resulting from a system restart is smoothed by the overall design convergence.

### *3.2. Design of a HLF nacelle*

In this section it is demonstrated how the Inverse Design System can be used within a realistic nacelle design process. The aim is to design a wing-mounted HLF nacelle (hybrid-laminar flow) at a higher free stream Mach number, i.e., at $M_\infty = 0.82$, than in the before mentioned nacelle redesign case. The concept of hybrid-laminar flow uses both boundary layer suction (up to a nacelle chord length of $x/c \approx 0.20$) and contouring of the nacelle in order to establish laminar flow at high transonic Mach numbers. In general, it is expected that a negative pressure gradient on the nacelle contour is able to establish a longer laminar boundary layer and therefore a lower total drag than a conventional nacelle. A typical HLF pressure distribution shows two acceleration peaks in the nose and mid-chord nacelle region. It should be mentioned that due to the inviscid flow regime within the flow field calculations it is not possible to evaluate if the boundary layer is really laminar. The term hybrid-laminar flow nacelle refers to the type of target pressure distribution only. The general aim of this section is to demonstrate the principle capability of the Inverse Design System to generate such type of nacelle shapes.

In a first step a nacelle contour is generated for an isolated nacelle. This approach gives the opportunity that for a limited numerical effort an intermediate nacelle contour can be designed which fulfills all major design constraints. As initial geometry the before mentioned conventional VHBR engine nacelle designed for a free stream Mach number of $M_\infty = 0.75$ is chosen. The angle of attack is $\alpha = 2.0°$.

Fig. 5 shows surface pressure distributions and nacelle profiles of the isolated HLF nacelle design in two circumferential sections at $\theta = 0°$ and 90° (corresponding to the

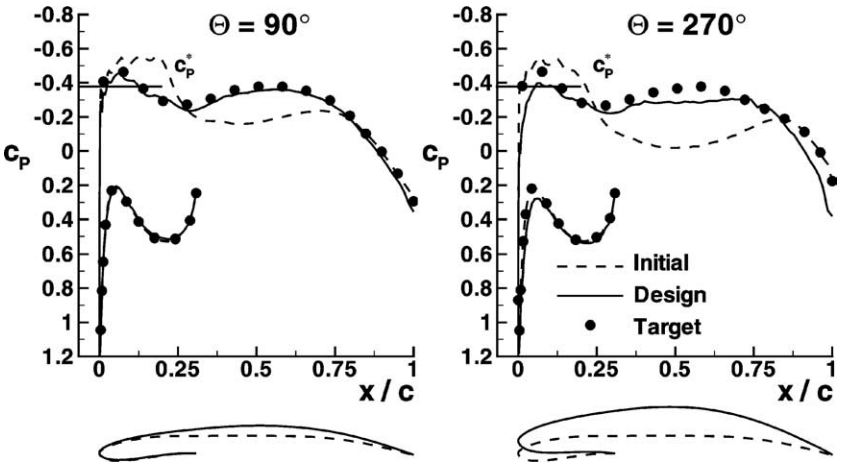


Fig. 6. Design of a wing-mounted HLF engine nacelle (intermediate result): surface pressure distributions and nacelle profiles.

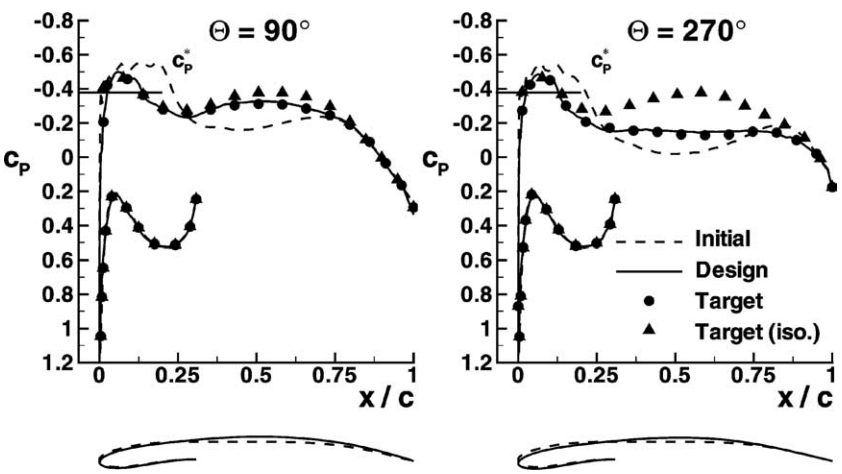


Fig. 7. Design of a wing-mounted HLF engine nacelle: surface pressure distributions and nacelle profiles.

top and the side section, respectively). As can be seen the target pressure distributions are precisely met. The acceleration at the nacelle leading edge reaches sonic velocities. The following deceleration should not be too strong in order to avoid the risk of flow separation due to the pressure rise. The second acceleration peak also reaches sonic velocities at $x/c \approx 0.50$ and therefore produces a favorable pressure gradient on the nacelle contour. Care has to be taken to avoid an extensive pressure rise at the rear end of the nacelle, where flow separation can occur, too.

The second step involves the design of a wing-mounted HLF engine nacelle. For this purpose, the final pressure distribution of the isolated HLF nacelle (see Fig. 5) is taken as target pressure distribution for the wing-mounted HLF nacelle design run. Doing so a contour is designed which fulfills the flow field requirements for a HLF nacelle while also taking into account the aerodynamic engine integration effects.

Fig. 6 shows surface pressure distributions and nacelle profiles in two circumferential sections at $\theta = 90°$ and 270° (corresponding to the outboard and the inboard section, respectively) as an intermediate design result. This nacelle design case can not be called successful since the calculated geometry changes are too extensive for a realistic nacelle contour. Especially in section $\theta = 270°$ the nacelle thickness increases by an unacceptable amount without matching the target pressure distribution. Due to the position of the initial nacelle under the wing a region of increasing pressure is present in the inboard section up to $x/c \approx 0.50$. Now, during the design process the target pressure distribution tries to establish the necessary negative pressure gradient for a laminar boundary layer by increasing the nacelle thickness.

The target pressure distribution of the isolated HLF nacelle design case has to be modified in order to design a realistic wing-mounted HLF nacelle. This means that the task of finding an adequate HLF pressure distribution has to be repeated partially. The example shows that it is absolutely necessary to include all aerodynamic effect in the design process. Performing only an isolated nacelle design bears the risk of a failure because the real flow physics around the final configuration is not taken into account properly.

Fig. 7 shows the result of the repeated wing-mounted HLF nacelle design. As can be seen, the target pressure distribution is changed compared to the isolated design case in

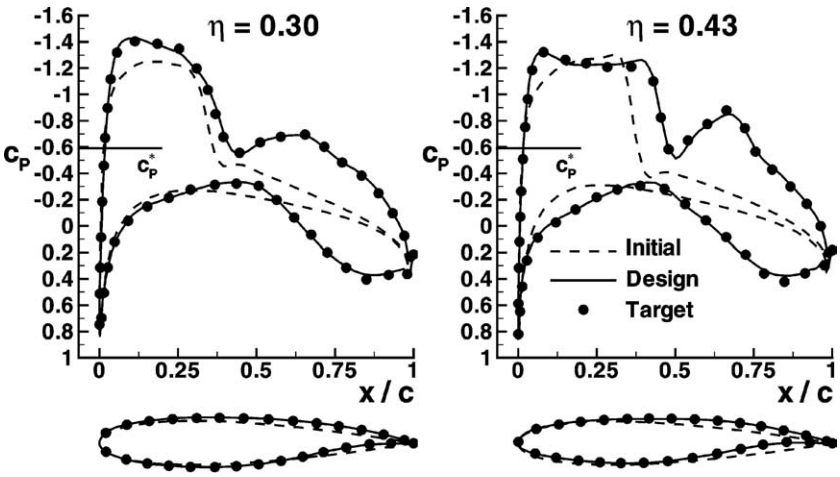


Fig. 8. Redesign of a transonic wing: surface pressure distributions and wing profiles.

order to produce a more realistic nacelle contour. The figure shows that it might not be possible to establish a laminar boundary layer in section $\theta = 270°$ because the necessary negative pressure gradient can not be fully established.

### 3.3. Wing redesign

In this section the Inverse Design System is applied to the design of a transonic wing. As before a redesign of an existing wing is performed. The configuration under consideration is the DLR ALVAST wing-fuselage configuration. The free stream parameters are $M_\infty = 0.75$ and $\alpha = 0.50°$. The start configuration of this redesign run is the ALVAST fuselage equipped with a wing built by NACA0012 profiles only. The wing twist distribution is kept constant. The target pressure distribution is taken from a flow field calculation of the original configuration.

Fig. 8 shows the result of the wing redesign case. In two spanwise sections at $\eta = 0.30$ and 0.43 it is shown that the target pressure distribution is met by the pressure distribution of the designed wing contour. This redesign case exhibits a distinct supersonic flow region on the wing upper side which can not properly be solved using the original Takanashi method. Therefore, it is necessary to increase the stabilizing upwind factor $D$ of Eq. (9) to a value of 10.0 in order to prevent a divergent design solution.

### 3.4. Reduction of engine integration effects

Another application demonstrates the ability of the Inverse Design System to focus more on the aerodynamic engine integration effects than on the pure design of a wing or a nacelle. For this purpose the DLR F6 configuration is used, a twin engine wide body transport aircraft model. The configuration is equipped with a long duct throughflow nacelle of CFM56 type which is closely-coupled to the wing. Due to the close coupling, the wing lower side inboard of the pylon is subjected to a narrow channel flow resulting in a strong shock on the surrounding wing, pylon, and nacelle surfaces.

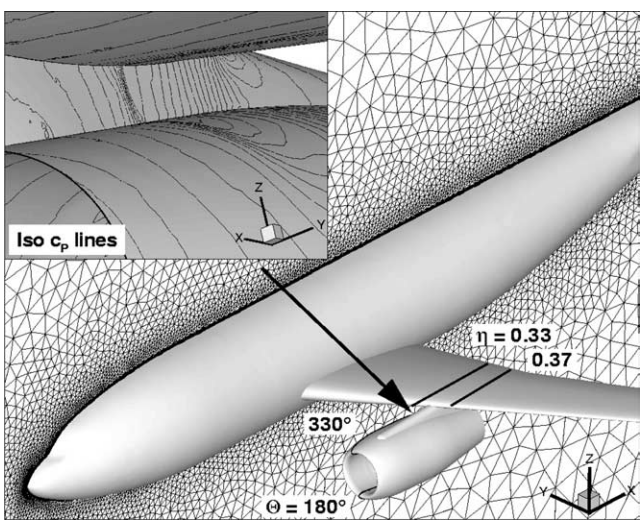


Fig. 9. DLR F6-CFM56 configuration.

Fig. 9 shows the F6 configuration at cruise conditions with lines of constant pressure in the wing, pylon, nacelle region.

In a first approach the shock in the wing, pylon, nacelle region should be eliminated by shaping the nacelle contour only. A nacelle target pressure distribution is defined which does not show a signature of the shock. The Inverse Design System is used to generate a nacelle contour which fulfills this pressure distribution. During the design iterations, inviscid flow field calculations are performed at a free stream Mach number $M_\infty = 0.75$ and an angle of attack of $\alpha = 0.85°$. A geometric constraint is applied such that the nacelle contour is changed at $x/c > 0.40$ only. The geometric constraint is enforced by setting the surface pressure differences $\Delta c_P$ and the calculated geometry differences $\Delta z$ explicitly to zero in regions where no geometry changes should take place. The smoothing of the calculated geometry differences including the constrained region with $\Delta z = 0.00$ ensures tangency at the junction of both regions.

Fig. 10 shows the result of this nacelle design in two circumferential sections. The section at $\theta = 180°$ shows

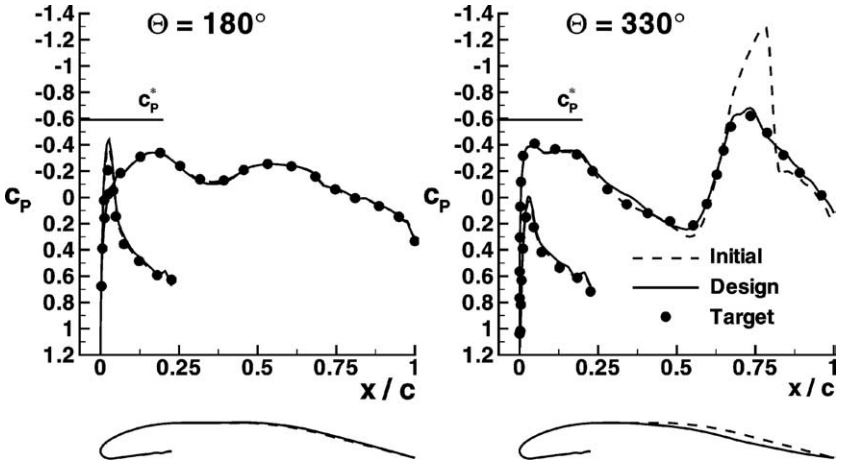


Fig. 10. Reduction of engine integration effects by nacelle contour shaping: surface pressure distributions and nacelle profiles.

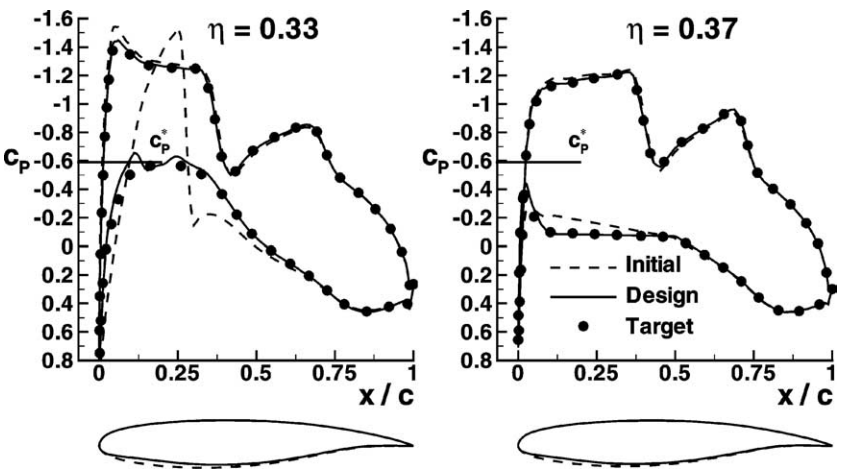


Fig. 11. Reduction of engine integration effects by wing contour shaping: surface pressure distributions and wing profiles.

no changes in the nacelle contour since nearly no aerodynamic installation effects take place in this region. In contrast, the pressure distribution of the initial nacelle contour at $\theta = 330°$ clearly shows the strong shock in the wing, pylon nacelle region. The prescribed target pressure distribution limits the maximum surface Mach number to a value of $M_{\text{local}} = 1.00$. As can be seen, the prescribed target pressure distribution is met. The designed contour is characterized by a reduced radius in the rear part of the nacelle.

In a second approach the shock in the wing, pylon, nacelle region should be reduced by changing the wing contour only. A wing target pressure distribution is generated which limits the maximum surface Mach number on the wing to a value of $M_{\text{local}} = 1.00$. The free stream parameters are the same as before. A geometric constraint is applied which allows wing contour changes only at $0.30 < \eta < 0.50$.

The result of this wing design is shown in Fig. 11. In two spanwise sections inboard and outboard of the pylon at $\eta = 0.33$ and 0.37 surface pressure distributions and wing cross sections are shown. As can be seen the prescribed target pressure distribution is reached in both sections. The shock on the wing lower side inboard of the pylon is substantially reduced. This has been established by a reduction of the thickness of the wing profile at $x/c < 0.50$.

The two examples in the preceding paragraphs have shown how the Inverse Design System can be used the reduce the aerodynamic engine integration effects on the DLR F6 CFM56 configuration. Nevertheless, due to the fact that within the design iterations inviscid flow field calculations are performed only it is not possible to quantify the aerodynamic benefit of the new designs in terms of total drag reduction. Therefore, viscous flow field computations are carried out for the original and the modified configurations.

Fig. 12 shows wing pressure distributions in two spanwise locations at $\eta = 0.33$ and 0.37 for the initial F6 CFM56 configuration and three modified configurations (by contour changes of nacelle or wing only, or both). The surface pressure distributions are gained by viscous flow field calculations using the DLR TAU Code and the Spalart–Allmaras turbulence model with Edwards modification [7]. The initial hybrid grids used consist of approximately 2.3 million grid points and are adapted twice with respect to $y^+$ and the flow field solution. For the design cruise Mach number of $M_\infty = 0.75$ the targeted lift coefficient is set to $C_L = 0.50$.

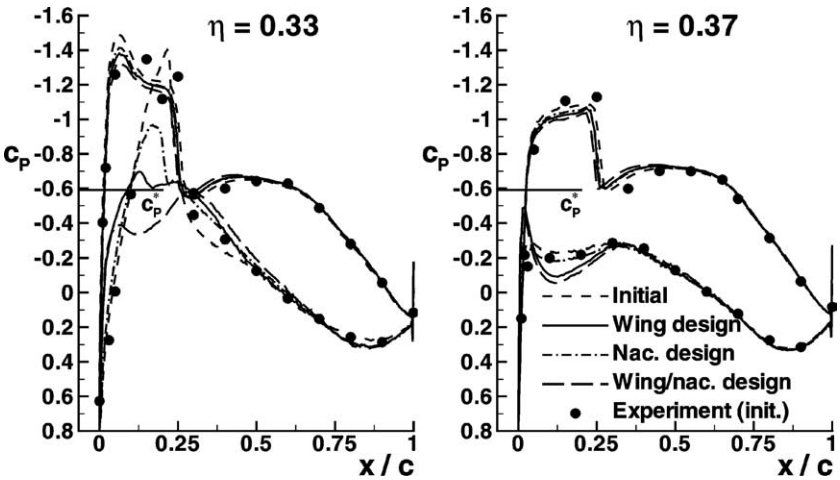


Fig. 12. Viscous flow field calculations of the F6 CFM56 configuration: surface pressure distributions.

Table 1
Viscous flow field calculations of the F6 CFM56 configuration (initial and modified): total coefficients

| Case | $C_L$ | $C_D$ | $\alpha$ |
|---|---|---|---|
| Initial | 0.500 | 0.0323 | 0.825° |
| Wing design | 0.500 | 0.0318 | 0.765° |
| Nac. design | 0.499 | 0.0318 | 0.788° |
| Wing/nac. design | 0.500 | 0.0315 | 0.740° |
| Experiment | 0.498 | 0.0340 | 1.030° |

The Reynolds number based on the aerodynamic mean chord length is $\mathrm{Re} = 3 \times 10^6$. As comparison, experimental data of a test campaign performed in the ONERA S2MA wind tunnel in 1993 is shown, too. Geometric differences appear between the wind-tunnel model and the numerical model since the numerical model does not include the wing deformation due to the aerodynamic loads.

The surface pressure distributions of the initial configuration show a good agreement with the experimental data. The supersonic region on the wing upper side is underpredicted by the numerical results. The locations of the shocks on both the wing upper and lower side match the experimental data well. The surface pressure distribution of the nacelle design case clearly shows the reduced shock strength on the wing lower side at $\eta = 0.33$. The same can be examined for the wing design case where the shock on the wing lower side is even further reduced. The combination of both modified components (wing and nacelle) into one configuration yields to the most extensive shock reduction on the wing lower side. The resulting total drag coefficients of the different configurations are given in Table 1. The separate wing or nacelle design cases achieve a total drag reduction of 5 drag counts ($dc = 10^{-4}$), respectively, whereas the combination of both components of the wing and nacelle design cases achieves a reduction of 8 drag counts.

## 4. Conclusions

An algorithm for the iterative inverse design of engine nacelles and wings has been presented. The method uses a residual-correction type approach to design a component surface which fulfills a prescribed target pressure distribution. The presented Inverse Design System uses the DLR flow solver TAU for the flow field calculation on unstructured grids.

The results presented show that the method is capable of designing engine nacelles and wings under influence of a complex aircraft configuration. Redesign test cases demonstrate the complete design functionality for engine nacelles and wings. A design of a HLF nacelle shows an application without an a-priori known solution. The example shows that for a successful design it is necessary to include all aerodynamic effects within the design process. A methodology is derived for the aerodynamic design of aircraft components. A second group of applications demonstrates the ability of the method to reduce aerodynamic engine integration effects by nacelle or wing contour modifications. The modified configurations result in performance gains of up to 8 drag counts compared to the total drag of the initial configuration. Compared to other known design algorithms, and depending on the numerical effort applied to a specific design task, the method presented offers the opportunity to efficiently include all aerodynamic effects during the design of complex aircraft configurations.

Future work should focus on further improvements for the specification of design constraints such that specific geometric values (e.g., minimum thickness) can be prescribed. New applications of the Inverse Design System like the design of pylon shapes or an aircraft's empenage should be considered, too.

## References


[1] W. Bartelheimer, An improved integral equation method for the design of transonic airfoils and wings, AIAA Paper 95-1688, 1995.

[2] R.A. Bell, R.D. Cedar, An inverse method for the aerodynamic design of three-dimensional aircraft engine nacelles, in: G.S. Dulikravich (Ed.), Proc. 3rd Int. Conference on Inverse Design Concepts and Optimization in Engineering Sciences, Washington, DC, 1991, pp. 405–417.

[3] O. Brodersen, M. Hepperle, A. Ronzheimer, C.-C. Rossow, B. Schöning, The parametric grid generation system MegaCads, in: B.K. Soni, et al. (Eds.), Proceedings of the 5th Intern. Conference on Numerical Grid Generation in Computational Fluid Dynamics and Related Fields, 1996, pp. 353–362.

[4] R.L. Campbell, L.A. Smith, A hybrid algorithm for transonic airfoil and wing design, AIAA Paper 87-2552, 1987.

[5] R.L. Campbell, Efficient viscous design of realistic aircraft configurations, AIAA Paper 98–2539, 1998.

[6] CentaurSoft, The grid generation package Centaur, http://www.centaursoft.com, 2004.

[7] J.R. Edwards, S. Chandra, Comparison of eddy viscosity-transport turbulence models for three-dimensional, shock-separated flowfields, AIAA J. 34 (4) (1996) 756–763.

[8] I. Fejtek, D. Jones, G. Waller, E. Hansen, S. Obayashi, A transonic wing inverse design capability for complete aircraft configurations, AIAA Paper 2001-2443, 2001.

[9] P. Garabedian, G. McFadden, Design of supercritical swept wings, AIAA J. 20 (3) (1982) 289–291.

[10] T. Gerhold, O. Friedrich, J. Evans, M. Galle, Calculation of complex three-dimensional configurations employing the DLR TAU-code, AIAA Paper 97-0167, 1997.

[11] W.F. Lin, A.W. Chen, E.N. Tinoco, 3D transonic nacelle and winglet design, AIAA Paper 90-3064, 1991.

[12] J.B. Malone, J. Vadyak, L.N. Sankar, A technique for the inverse aerodynamic design of nacelles and wing configurations, AIAA Paper 85-4096, 1985.

[13] K. Matsushima, S. Takanashi, An inverse design method for wings using integral equations and its recent progress, in: K. Fuji (Ed.), in: Notes on Numerical Fluid Mechanics, vol. 68, 1999, pp. 179–209.

[14] D.A. Naik, S.E. Krist, R.L. Campbell, V.N. Vatsa, P.G. Buning, L.M. Gea, Inverse design of nacelles using multi-block Navier–Stokes codes, AIAA Paper 95-1820, 1995.

[15] S. Takanashi, Iterative three-dimensional transonic wing design using integral equations, J. Aircraft 22 (8) (1985) 655–660.

[16] R. Wilhelm, Inverse design method for designing isolated and wing-mounted engine nacelles, J. Aircraft 39 (6) (2002) 989–995.